24 February 1995

ELSEVIER

Chemical Physics Letters 233 (1995) 500–508

CHEMICAL PHYSICS LETTERS

Femtochemistry of organometallics: dynamics of metal–metal and metal–ligand bond cleavage in $M_2(CO)_{10}$

Sang Kyu Kim, Soren Pedersen, Ahmed H. Zewail

Arthur Amos Noyes Chemical Physics Laboratory [1], California Institute of Technology, Pasadena, CA 91125, USA

Received 30 December 1994

Abstract

We report femtochemical studies of the organometallic dimetal decacarbonyl. By the use of mass spectrometry, we obtain the temporal dynamics in the channels for metal–metal and metal–ligand bond cleavage. The time scale observed for cleavage and for structural bridging indicates the nature of the repulsion along the two reaction coordinates and the interplay between the bond order and the femtosecond dynamics.

1. Introduction

Organometallic compounds have unique functions and properties which are totally determined by the dynamics of metal–metal (M–M) and metal–ligand (M–L) bonding [1,2]. The time scales for such cleavage determine the product yield and the selectivity in the product channel. It also establishes the nature of the reactive surface: ground-state versus excited-state chemistry.

One class of reactions which has been the subject of detailed spectroscopic, mechanistic, and theoretical studies is the carbonyl containing metal–metal compounds (for recent reviews, see Refs. [3,4]). For these compounds it is known that both the M–M and M–CO bonds can be broken upon UV excitation. There have been numerous studies aimed at understanding the dissociation mechanism of these metal complexes in solutions as well as in the gas phase. The energetics, spectroscopy, and photochemistry of these metal complexes have also been extensively studied.

For dimetal and related complexes, several aspects of the dissociation mechanism have been addressed, starting with the assignment of the optical transitions [5]. The primary photodissociation channels [6–11] and their time scales for dissociation [8,12–16] have been examined. The bond energies and internal energy distributions of photoproducts [8,17–19], molecular rearrangement and bridging [20–22], and solvent complexation and vibrational relaxation in solutions [13–15,23] have also been studied by many groups.

On the theoretical side, there has been significant progress in understanding the electronic structure of these and related systems [24,25]. The molecular electronic structure [26] and correlation diagrams [27] of the reactive channels have been described. Molecular dynamics studies by the Manz group [28,29] on related systems have determined the elementary time scale for metal–ligand bond breakage

[1] Contribution No. 9032.

0009-2614/95/$09.50 © 1995 Elsevier Science B.V. All rights reserved
SSDI 0009-2614(95)00050-X

and exploited these femtosecond (fs) time scales to control the outcome of reactions.

In this Letter, we report the first studies of the fs dynamics of isolated $Mn_2(CO)_{10}$ in a molecular beam. The goal is to directly obtain the cleavage time for the M–M and M–CO bonds and to examine the mechanism in relation to bonding characteristics. Since these studies are carried out in a molecular beam, complications from solvent caging of ligands and possible cooling by vibrational relaxation can be eliminated. Hence, direct comparison with theory could be made. To date most measurements (see below) have provided an upper limit of a few picoseconds. However, it is important to resolve the elementary motion in order to compare the dynamics in the two channels and to establish whether the dissociation takes place on the excited surface, or on the ground state reached by intramolecular vibrational-energy redistribution (IVR).

In the gas phase, the time scale of dissociation in these and related systems were obtained, as an upper limit, using two different approaches: Measurement of the anisotropy parameter (β) and the fluence dependence of ionization yield. Bersohn's group [8] reported the first collision-free gas-phase photodissociation study for $Mn_2(CO)_{10}$ and $Re_2(CO)_{10}$. From measurement of $\beta \approx 1.9$ (for $Mn_2(CO)_{10}$) they deduced an upper limit of 2–3 ps for the lifetime (from calculation of the rotational period). In this same study, they showed that M–M fragmentation is the primary channel. In a subsequent study, Vaida's group [10] showed that both the M–M and M–CO fragmentation channels are active. Grant's group [12] used the fluence dependence of ionization versus fragmentation in supersonic jets and again deduced an upper limit for the dissociation time (≈ 1 ps) in the case for $Fe(CO)_5$.

Nelson's group studied the M–CO bond cleavage in $M(CO)_6$, where M = Cr, Mo, and W [14], in solution using fs laser pulses, and reported a dissociation time of less than ≈ 500 fs. From their experiments, also in solution, Harris' group obtained an upper limit of the dissociation time (actually referred to as predissociation) of 2–3 ps or less [13]. In a later study the results for the photolysis of $Mn_2(CO)_{10}$ were interpreted in terms of ultrafast geminate recombination which occurs on a ≈ 350 fs time scale, predominantly by a single collision with the surrounding solvent cage [16]. This analysis of the results in solution suggests a shorter time scale for the primary dissociation channel. Recently, the group of Ruhman observed coherent photodissociation, using fs pulses, and provided a simplified molecular orbital scheme for the decarbonylation [15].

The absorption spectrum of $Mn_2(CO)_{10}$ in cyclohexane is very broad and does not give dynamical information. The spectrum shows that the maximum extinction coefficient is at ≈ 345 nm and that the transition can be assigned as $\sigma \rightarrow \sigma^*$ promotion along the Mn–Mn bond, Fig. 1 [5,13]. The $\sigma \rightarrow \sigma^*$ transition removes the bonding character of the Mn–Mn bond and leads to the dissociation into two $\cdot Mn(CO)_5$ products. According to a state-correlation diagram, two $\cdot Mn(CO)_5$ product states correlate with the lower-lying triplet, excited state, which could be directly accessed either by the optical excitation or through intersystem crossing from the excited singlet state [3,27]. The other absorption transitions, peaking near ≈ 260 and ≈ 300 nm, have been assigned to metal-to-ligand charge transfer (MLCT) transitions, which correspond to $d\pi \rightarrow \pi^*(CO)$ and $\sigma \rightarrow \pi^*(CO)$ transitions, respectively [5]. These transitions tend to weaken the metal–ligand bond and could lead to Mn–CO bond breakage. However, the mechanism describing the dynamics of elementary bond dissociation could not be resolved from the spectra.

In this work, we examine the elementary dissociation dynamics of $Mn_2(CO)_{10}$ and provide a direct measurement of the M–M and M–CO bond cleavage, free of the solvent. From these results we describe the mechanism for the reaction in the two channels. The products of $Mn_2(CO)_{10}$ in the molecular beam were detected by time-of-flight (TOF) mass spectrometry with fs time resolution. Two primary channels were distinguished by detecting Mn^+ from $\cdot Mn(CO)_5$ and Mn_2^+ from $Mn_2(CO)_9$ (Fig. 1). On the fs time scale, the primary steps could be isolated, as ionization is observed before fragmentation. The time scale for the cleavage provides a dynamical picture which is correlated with the nature of the M–M and M–CO bond potentials. We also relate the observed long-time behavior of the Mn_2^+ transient to the molecular rearrangement of the $Mn_2(CO)_9$ product to form a 'bridged' complex, a process studied in low-temperature matrices [21,22], and on the basis of

solution-phase studies thought to occur within a picosecond [15].

2. Experimental

The system for the generation of the fs laser pulses has been described in detail elsewhere [30]. Briefly, the 514.5 nm output of an Ar^+ laser (Coherent, 2.8–3.0 W) pumped a colliding-pulse mode-locked (CPM) ring dye laser to generate ultrafast laser pulses at $\lambda_{max} \approx 620$ nm with an 83 MHz repetition rate. The pulses from the CPM laser were amplified by a four-stage pulsed dye amplifier (PDA) pumped by a Nd:YAG laser (Spectra Physics DCR3) with a 20 Hz repetition rate. The amplified pulses were recompressed by prism pairs and split into two pulses for use as clocking pump and probe. The laser pulse for the pump was focused into a KD*P crystal (0.5 mm thick, type I) to generate the frequency-doubled output with a peak at 310 nm. The 620 nm probe was delayed with respect to the pump by a retro-reflector on a computer-controlled actuator. The pulse length of the final output of the laser system was ≈ 85 fs (fwhm) measured by autocorrelation. The spectral width was measured to be ≈ 7 nm for 620 nm. The laser pulses were recombined collinearly by a dichroic mirror and focused into the molecular beam chamber.

The molecular beam chamber had a two-stage pumping system divided by the ≈ 2 mm diameter skimmer, Fig. 2. The sample, $Mn_2(CO)_{10}$ (98% assay, Strem Chemicals), was heated to 45–50°C and seeded in He carrier gas with a typical backing pressure of ≈ 20 psi. The background pressure in the ionization TOF chamber was maintained at $\approx 3 \times 10^{-6}$ Torr when the nozzle (0.3 mm diameter) was open. The nozzle temperature was set at ≈ 5°C higher than the sample holder to prevent condensation inside the nozzle. Diethylaniline (DEA) was purchased from Aldrich (98% assay) and used without further purification.

The products following excitation of $Mn_2(CO)_{10}$ were ionized by the probe fs laser pulse. The ions formed were repelled, accelerated, and allowed to drift through the field-free region before being detected by micro-channel-plates (MCP). The TOF mass spectrum was taken using a transient digitizer

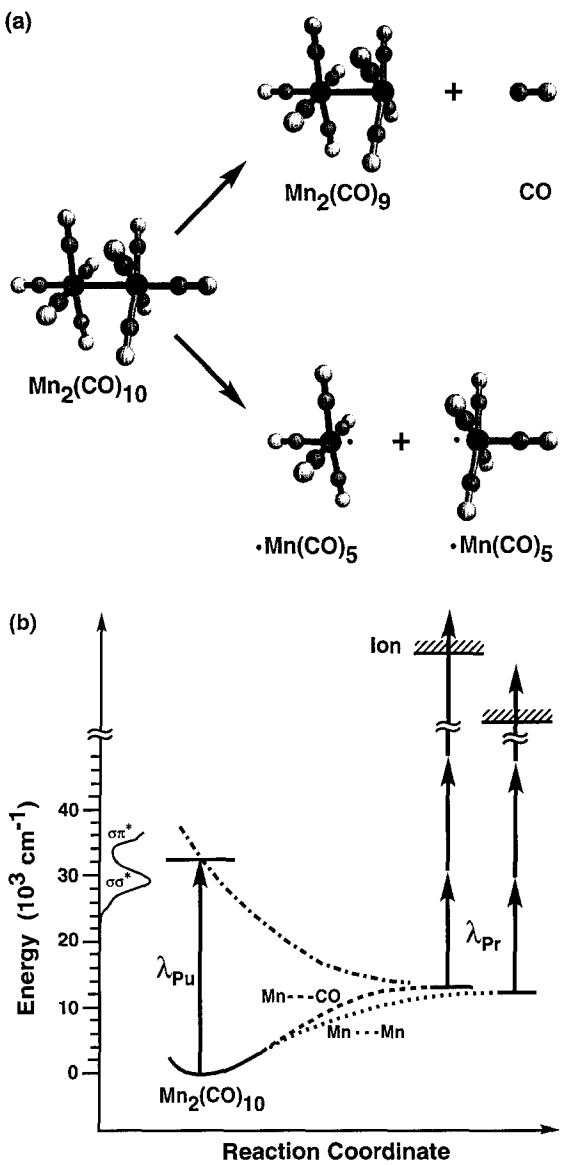

Fig. 1. (a) Molecular structures and bond cleavage in the two channels leading to $Mn_2(CO)_9$ and $\cdot Mn(CO)_5$. (b) Energetics of the scheme for probing the fragmentation dynamics in the two channels along the metal–metal (Mn–Mn) and the metal–ligand (Mn–CO) bond. The absorption spectrum shown here is taken in solution [13] and bond energies are from solution phase studies [13,18,19].

(LeCroy 8818A). The fs transient for a specific mass was obtained using a boxcar integrator (SR250) and monitoring the selected ion signal as a function of the delay time between the pump and probe laser pulses. Each data point was averaged for 3 laser

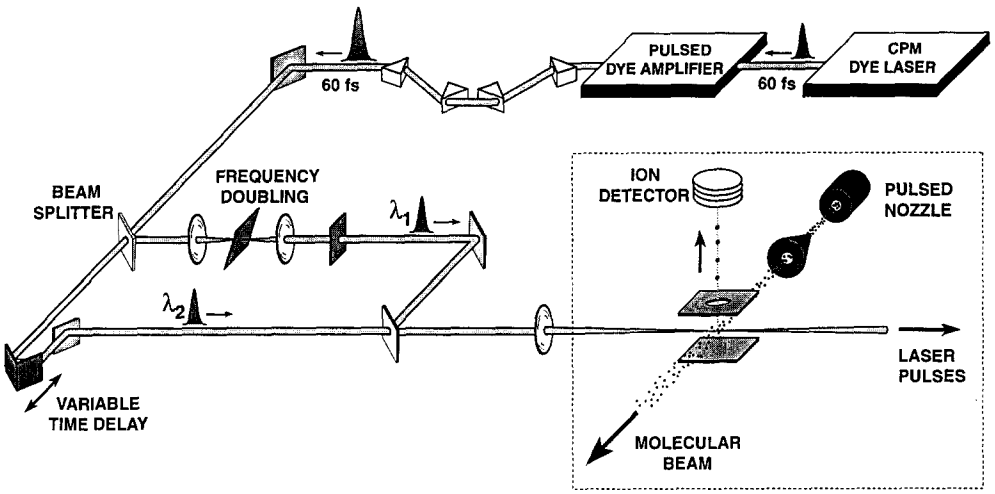

Fig. 2. The experimental setup, showing the generation of femtosecond laser pulses. The probe pulse (λ_2) is delayed with respect to the pump pulse (λ_1) by a computer-controlled actuator. The two pulses were made to travel collinearly and focused onto the molecular beam. Ions are detected in the time-of-flight mass spectrometer.

shots, and the transients were accumulated for over 100–300 scans to achieve a signal-to-noise ratio of at least 10–20.

3. Results and discussion

The TOF mass spectrum of $Mn_2(CO)_{10}$ taken with fs pulses at 310 nm is shown in Fig. 3. Two main peaks, Mn^+ and Mn_2^+, were observed, which are consistent with the mass spectra reported earlier [10,31]. Other species such as $Mn_2(CO)_{10}^+$, $\cdot Mn(CO)_5^+$, and $Mn_2(CO)_4^+$ could also be observed, but with weaker intensities. The distribution of ion fragmentation is known to depend on the wavelength and the intensity of laser pulses [31,32].

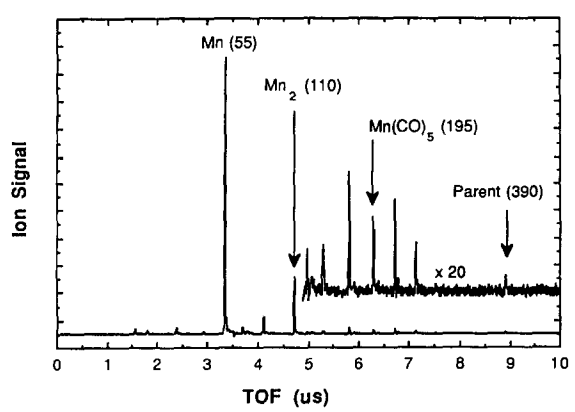

Fig. 3. The time-of-flight (TOF) mass spectrum of $Mn_2(CO)_{10}$ taken with femtosecond laser pulses at 310 nm.

A pump and probe intensity-dependence study was performed on the Mn^+ signal. A log–log plot of the Mn^+ signal versus the laser intensity gave a number close to unity for the pump laser and significantly larger than unity for the probe laser. This indicates that excitation by the pump laser is predominantly a one-photon absorption process, while ionization by the probe laser requires a multiphoton process, consistent with the scheme in Fig. 1. The multiphoton excitation by the probe laser involves dissociation and ionization, and the evaporation of all CO ligands in the process of probing is due to both processes [31,32], depending on the time scale and the fluence.

Transients for $Mn_2(CO)_{10}^+$, Mn_2^+, Mn^+ are shown with the fits in Fig. 4. Here, the pump and probe laser intensities were so weak that there was no ion signal due to either pump or probe laser alone. The Mn^+ and Mn_2^+ transients were taken at the pump intensity where the Mn^+ signal is linear with the pump laser intensity. For the $Mn_2(CO)_{10}^+$ transient, since the signal was so weak, the pump intensity was increased from that used for Mn^+ and Mn_2^+. The pump laser was polarized parallel to the TOF detec-

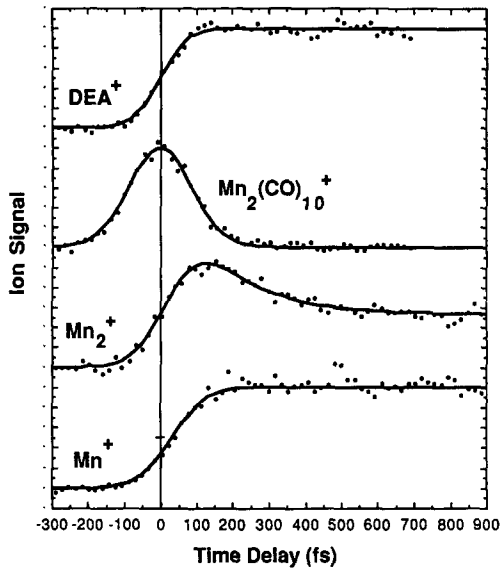

Fig. 4. Femtosecond transients of $Mn_2(CO)_{10}^+$, Mn_2^+, and Mn^+, and for calibration DEA^+. The fits are shown as solid lines. The solid vertical line indicates time-zero at which there is no delay between the pump and probe pulses. The Mn_2^+ transient was fit with a decay time of 160 fs to the asymptote.

tion axis, and the probe laser polarization was at 54.7° to that of the pump. This is not necessarily the magic angle [33]. If this was close to the magic angle, this setup gives transients which are not affected by the rotational motion of the fragment for which the recoil vector was initially aligned by the pump laser polarization [34].

The transient for DEA^+ in the molecular beam was taken with the exact same conditions and displayed in Fig. 4. Time-zero is defined as the middle of the rise of the DEA^+ transient. As expected, this corresponds to the peak of the $Mn_2(CO)_{10}^+$ transient. The transients for $Mn(CO)_5^+$ and $Mn_2(CO)_4^+$ were also recorded, and these are very similar to the $Mn_2(CO)_{10}^+$ transient, indicating their origin from the parent.

The Mn_2^+ transient shows an apparent peak shift of ≈ 100 fs, while the Mn^+ transient shows a shift to a plateau of ≈ 150 fs. More quantitative fits indicate that the initial rise in both Mn^+ and Mn_2^+ transients is similar to the calibration transient of DEA^+. The Mn^+ transient shows the initial rise to the plateau and the signal remains constant for more than ≈ 100 ps. Meanwhile, the Mn_2^+ transient displays the initial rise to the peak and a decay (≈ 160 fs) to an asymptotic level where it then remains constant for more than ≈ 100 ps.

The polarization anisotropy as a function of the delay time, $r(t)$, was also measured for both Mn^+ and Mn_2^+ transients. The $r(0)$ was nearly ≈ 0.4 for both ions, consistent with the initial transition involved being parallel to the molecular axis [34]. The $r(t)$ shows an exponential fit with a characteristic time of ≈ 700 fs for the Mn^+ transient and ≈ 100 fs for the Mn_2^+ transient. This large difference in the $r(t)$ for the two transients provides information about rotations in fragmentation as well as about changes in the transition moment due to rearrangement of the molecular structure, as discussed below.

3.1. Femtosecond mass spectrometry of the two channels

The transients obtained by mass detection of ions reflect the dynamics of the parent $Mn_2(CO)_{10}$ or the nascent $\cdot Mn(CO)_5$ and $Mn_2(CO)_9$ products. Fragmentation in the ion channel does not influence such measurements since fs resolution enables one to observe ionization prior to fragmentation [30]. The $Mn_2(CO)_{10}^+$ transient in Fig. 4 indicates an ultrashort lifetime of the excited parent molecule, which decays completely in less than ≈ 85 fs, our fs pulse width. The Mn^+ and Mn_2^+ transients do not show this fs decay component, and hence represent the dynamics of the nascent products, $\cdot Mn(CO)_5$ and $Mn_2(CO)_9$.

The Mn_2^+ transient arises from $Mn_2(CO)_9$ and not from the $\cdot Mn(CO)_5$ product; note that from the energetics in Fig. 1, the available energy is sufficient to decarbonylate one CO and at most two. The peak of the Mn_2^+ transient is shifted by ≈ 100 fs from the time-zero (Fig. 4), while the Mn^+ transient does not have any corresponding peak, indicating that it represents the dynamics of the other nascent product, $\cdot Mn(CO)_5$. This is consistent with the fragmentation and ionization pathways. First, neutral Mn_2 species, even if fragmented by the probe (or in free flight) to give an Mn^+ species, will display the same fs transient, whether detecting Mn^+ or Mn_2^+. This is not the case in our experiment, indicating that the Mn^+ and Mn_2^+ signals are from two different neutral channels. Second, a secondary pathway for an Mn species is in principle possible from a Mn_2 neutral

species. For example, the nascent vibrationally hot $Mn_2(CO)_9$ may dissociate into $\cdot Mn(CO)_5$ and $\cdot Mn(CO)_4$, and these species could be ionized to give the Mn^+ signal. However, the dissociation of vibrationally hot product requires IVR on the ps time scale. Therefore, the transients presented here reflect the dynamics of the neutral two channels (Fig. 1). This is consistent with previous photofragment spectroscopic studies [8,10].

The preference of Mn_2^+ over Mn^+ in probing the $Mn_2(CO)_9$ product can be understood on the basis of the strengthening of the M–M bond upon CO elimination. The strength of the M–M bond increases with CO elimination, thus reducing the M–M bond cleavage during probing. This also accounts for the formation of the bridged complex in the $Mn_2(CO)_9$ product. The Mn–Mn bond distance in $Mn_2(CO)_{10}$ is relatively long (≈ 3.0 Å) [26], and there is no evidence of bridging in $Mn_2(CO)_{10}$. There is, however, some experimental evidence for the formation of the bridged $Mn_2(CO)_9$ product upon UV excitation [21,22].

Finally, it should be emphasized that the absorption maximum found in solutions is at ≈ 500 nm for $Mn_2(CO)_9$ and ≈ 800 nm for $\cdot Mn(CO)_5$ [9], and accordingly the probe wavelength used here (620 nm) is between absorption maxima of the two fragments. If the probe wavelength is chosen in favor of one of these two absorptions, then the Mn^+/Mn_2^+ transients would also reflect such changes in the dynamics.

3.2. Metal–metal bond cleavage

The $\sigma \rightarrow \sigma^*$ transition of the Mn–Mn bond reduces the bond order to zero and therefore leads to the repulsive dissociation of $Mn_2(CO)_{10}$ along this bond. But the electronic states of $Mn_2(CO)_{10}$ are complex, and the upper electronic states involved in the optical excitation and dissociation are not yet totally certain [3,4]. According to a simple state-correlation diagram, the optically allowed singlet $^1(\sigma\sigma^*)$ state does not correlate to the ground state of two $\cdot Mn(CO)_5$ products. The lower-lying triplet $^3(\sigma\sigma^*)$ state to which an optical transition is spin-forbidden, in a zeroth-order approximation, could make such a correlation [3,27]. Therefore, dissociation along the M–M bond occurs on the $^3(\sigma\sigma^*)$ state accessed either through the intersystem crossing (ISC) from the optically prepared $^1(\sigma\sigma^*)$ state or by the direct excitation due to strong spin–orbit coupling.

The time shift observed for the Mn^+ signal is measured to be ≈ 40 fs halfway up on the rise (Fig. 4). This observation of a fs shift excludes the possibility that the cleavage is due to predissociation. It also excludes ground-state dissociation since the time is too short for internal conversion and IVR to be effective. Because of its impulsive nature, we conclude that the mechanism of the cleavage must involve a dissociative, repulsive potential-energy surface, accessed directly (i.e. $^3\sigma\sigma^*$) or reached by very large non-adiabatic ISC ($^1\sigma\sigma^*/^3\sigma\sigma^*$). It is interesting to note that, in the first quantum simulation [28], Manz and co-workers have shown that direct dissociation of $HCo(CO)_4$ to H and $Co(CO)_4$ takes 20 fs while the indirect ISC takes 50 fs.

For fragmentation on the repulsive surface, the shift represents the time for the two fragments to move beyond their force field of interaction. In analogy with direct dissociation reactions [35], we can deduce the nature of the repulsive potential and its interaction length from knowledge of the bond energy, the available energy and the reduced mass. The Mn–Mn bond energy in the gas phase is still not certain, and different values ranging from 22 to 42 kcal/mol have been reported [17]. Assuming a value of D(Mn–Mn) ≈ 36 kcal/mol [18], which has been determined in solution, the available energy is then ≈ 56 kcal/mol at the pump wavelength of ≈ 310 nm. If all the available energy is transformed to kinetic motion of the fragments, the upper limit for the recoil velocity is ≈ 0.022 Å/fs. Accordingly, for ≈ 40 fs of delay time, the separation between centers of masses of the two $\cdot Mn(CO)_5$ fragments must be ≈ 0.9 Å from the equilibrium distance.

For a one-dimensional repulsive potential, $V(R) = E \exp[-(R - R_0)/L]$, for two fragments at separation (R), the length parameter (L) can be determined from a simple relationship relating the time shift to the recoil velocity and total energy [30]. For the Mn–Mn cleavage we obtained $L \approx 0.2$ Å, indicating a very steep potential for repulsion in the σ^* charge density. From experiments carried out in the gas phase and in solution [3,8], the $\cdot Mn(CO)_5$ product has actually been found to be vibrationally hot,

indicating that L could be even less than 0.2 Å. Furthermore, the reaction coordinate for the Mn–Mn bond cleavage cannot be simply described as the elongation of the distance between two 'frozen' fragments. It should include other vibrational motions (e.g. those involving CO ligands) as the ultrafast repulsion between the metal atoms changes with time. A more accurate determination of the Mn–Mn bond energy along with the information about the time delay and internal energy distributions at different energies would be very helpful for a complete picture of the molecular dynamics. Theoretical studies now should be of interest.

3.3. Metal–ligand bond cleavage

As mentioned above, the transient for Mn_2^+ probing can be simulated with a smaller time shift of ≈ 20 fs and a decay of ≈ 160 fs. This fs and very short delay observed for the Mn_2 species again excludes a predissociative or ground-state reaction mechanism. If the dynamics of this metal–ligand cleavage involves an initial bound $\sigma\sigma^*$ transition, then a non-adiabatic but strong crossing to a Mn–CO repulsive state must be involved. Waldman et al. [15] suggested that following the excitation of the molecule to the $(\sigma\sigma^*)$ state a non-adiabatic coupling to other electronic states will lead to cleavage of the Mn–CO bond. The direct transition to the $\pi^*(CO)$ orbital can also lead to rupture of the Mn–CO bond [13]. Actually, as shown in Fig. 1, at the pump wavelength of 310 nm, the transitions to both σ^* and $\pi^*(CO)$ are optically accessible. The fs appearance of the Mn_2^+ signal supports the mechanism that the Mn–CO bond cleavage *effectively* occurs on a repulsive, dissociative potential energy surface along the Mn–CO reaction coordinate, Fig. 5. It is interesting to note that this type of decarbonylation has been studied theoretically by Manz and co-workers for e.g. in $H_2Fe(CO)_4$ and found to occur in ≈ 100 fs [29].

The Mn–CO cleavage is faster than Mn–Mn cleavage and this is consistent with the kinematics. For the same amount of available energy, the recoil velocity for the Mn–CO bond dissociation is expected to be about 2 times higher than that for the Mn–Mn bond cleavage. This is because the reduced mass for the former is ≈ 4 times smaller than that

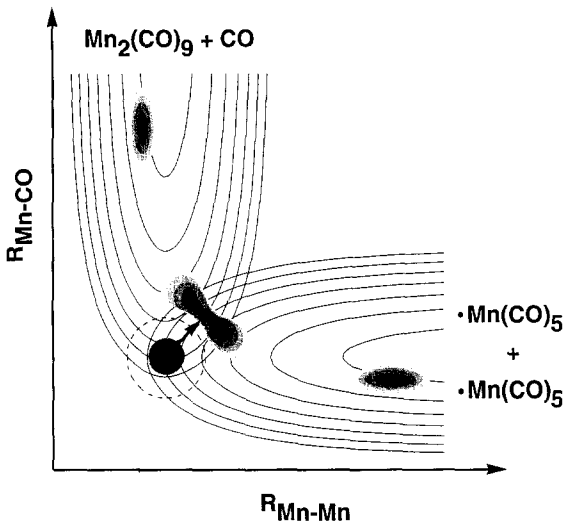

Fig. 5. Proposed scheme for the dynamics of bond cleavage in $Mn_2(CO)_{10}$. The direct excitation to the dissociative potential energy surfaces lead to fs bond ruptures along the M–M and M–L reaction coordinates. Both the diabatic and adiabatic (note the dotted circle) surfaces are shown, along with the wave packet motion along the two coordinates.

for the latter. Hence, a time-shift in the Mn_2^+ transient is expected to be ≈ 2 times less than that in the Mn^+ transient if the dissociative potential energy curves for both channels are of the similar nature. This simple picture is entirely consistent with our findings. In solution the Mn–CO bond energy is estimated to be ≈ 38 kcal/mol [19], which is comparable to the value of ≈ 36 kcal/mol for the Mn–Mn bond energy [18]. For the available energy of ≈ 54 kcal/mol, an upper limit for the recoil velocity is ≈ 0.042 Å/fs for Mn–CO. This is about twice the Mn–Mn bond recoil velocity. This again is consistent with the experimentally measured time shift of ≈ 20 fs for the Mn–CO bond cleavage compared to the ≈ 40 fs for the Mn–Mn bond.

The Mn_2^+ transient shows an initial rise to a maximum and a decay to an asymptote with a characteristic time constant of ≈ 160 fs (see Fig. 4). This decay reflects the change of nascent $Mn_2(CO)_9$ in the first few hundred fs. We now consider two pathways, one of which is the molecular rearrangement to form a bridged $Mn_2(CO)_9$ and the other is a further dissociation of vibrationally hot $Mn_2(CO)_9$

product. Both of these product channels have been studied by transient IR in solutions and matrices [11,21,22]. The dissociation process is less likely though because the time constant is too short for the vibrationally hot $Mn_2(CO)_9$ product to undergo statistical energy redistribution. The other pathway, i.e. the ligand bridging, is consistent with this time scale since molecular rearrangement occurs on a very short time scale, leading to a significant change in the ionization cross section. In this case, our measured decay of 160 fs for bridging is consistent with the recent finding by Ruhman's group that this process occurs on $<$ 1 ps time scale [15].

The fast decay ($\approx$ 100 fs) in the anisotropy $r(t)$ observed for the Mn_2^+ signal is also consistent with the bridging of $Mn_2(CO)_9$. As the molecule rearranges, the cylindrical symmetry is reduced, and this leads to a decrease in the polarization anisotropy with a time constant comparable to that of intramolecular rearrangement. For $r(t)$ of the Mn^+ signal we observed a longer decay ($\approx$ 700 fs) and this could reflect the rotational dynamics of the $\cdot Mn(CO)_5$ fragment. Because these $r(t)$ measurements involve multiphoton ionization [33], these results will be analyzed more quantitatively in further studies.

4. Conclusions

In this contribution, we present our first direct measurement of the dynamics of M–M and M–L bond cleavage using fs time resolution and TOF mass spectrometry. Both bond cleavages in $Mn_2(CO)_{10}$ occur on the fs time scale, indicating that previous estimate of the upper limit (2–3 ps) from measurements of the anisotropy parameter in the gas phase is about two orders of magnitude longer than obtained here. The rotational period is too slow to be used as an internal clock for this heavy molecule!

The fs cleavage dynamics excludes ground state dissociation as the time scale is much shorter than most vibrational motions needed to complete internal conversion and IVR. It represents direct dissociation on repulsive surfaces involving both the M–M and M–L charge distributions. Although the initial transition is assigned as $\sigma\sigma^*$, the dynamics is controlled by the reduction in bond order introduced by the repulsion in these coordinates, surprisingly leading to a slower M–M than M–L bond breakage. We deduce a repulsive length of $\approx$ 0.2 Å (upper limit $\approx$ 0.9 Å).

We account for the disparity in the time scale for M–M and M–L breakage on the basis of simple kinematics. The reduced mass in the Mn–CO cleavage is $\approx$ 4 times smaller than that of the Mn–Mn and, hence, the CO product separates apart $\approx$ 2 times faster than does $\cdot Mn(CO)_5$ product. Unlike the Mn-species, which builds up and live for at least 100 ps, the Mn_2-species decays in $\approx$ 160 fs. We relate this decay to the bridging of the nascent $Mn_2(CO)_9$ product.

There are several implications of these new findings. First, the measurements in solutions, which in many cases showed a longer time scale, must include possible caging by the solvent and/or vibrational cooling on the time scale of the experiment. The M–L may appear slower than M–M dynamics in solutions simply because of the easier kinematics of caging for the former. Second, the potential energy surface is not predissociative, as previously inferred, since we do not observe ps dynamics for the isolated reaction. Finally, while the bonding characteristics in these very interesting systems may involve a simple description (e.g. $\sigma\sigma^*$) of 'bound' states, the dynamics clearly shows the strong repulsive nature of the force. We consider this as evidence of the strong interactions leading to the adiabatic picture in Fig. 5.

Future work will include studies of the energy dependence, the time-dependent anisotropy, the detection of different fragments, and the comparison with other systems. Preliminary studies of $Re_2(CO)_{10}$ and of kinetic energy time-of-flight (KETOF) have been made and will be published later. Molecular dynamics calculations will also be of interest.

Acknowledgements

This work was supported by a grant from the National Science Foundation. We wish to thank Professor J. Manz for stimulating and helpful correspondence, and Professor S. Ruhman for communicating his work.

References

[1] G.L. Geoffroy, M.S. Wrighton, Organometallic photochemistry (Academic Press, New York, 1979).
[2] J. Chaiken, ed., Laser chemistry of organometallics (Am. Chem. Soc., Washington, 1993).
[3] T.J. Meyer and J.V. Caspar, Chem. Rev. 85 (1985) 187, and references therein.
[4] W.E. Hollingsworth and V. Vaida, J. Phys. Chem. 90 (1986) 1235.
[5] R.A. Levenson and H.B. Gray, J. Am. Chem. Soc. 97 (1975) 6042.
[6] M.S. Wrighton and D.S. Ginley, J. Am. Chem. Soc. 97 (1975) 2065.
[7] J.L. Hughey IV, C.R. Bock and T.J. Meyer, J. Am. Chem. Soc. 97 (1975) 4440.
[8] A. Freedman and R. Bersohn, J. Am. Chem. Soc. 100 (1978) 4116.
[9] L.J. Rothberg, N.J. Cooper, K.S. Peters and V. Vaida, J. Am. Chem. Soc. 104 (1982) 3536.
[10] D.G. Leopold and V. Vaida, J. Am. Chem. Soc. 106 (1984) 3720.
[11] T.A. Seder, S.P. Church and E. Weitz, J. Am. Chem. Soc. 108 (1986) 7518.
[12] R.L. Whetten, K.-J. Fu and E.R. Grant, J. Chem. Phys. 79 (1983) 4899.
[13] J.Z. Zhang and C.B. Harris, J. Chem. Phys. 95 (1991) 4024.
[14] A.G. Joly and K.A. Nelson, Chem. Phys. 152 (1991) 69.
[15] A. Waldman, S. Ruhman, S. Shaik and G.N. Sastry, Chem. Phys. Letters 230 (1994) 110.
[16] B.J. Schwartz, J.C. King, J.Z. Zhang and C.B. Harris, Chem. Phys. Letters 203 (1993) 503.
[17] J.A.M. Simões, J.C. Schultz and J.L. Beauchamp, Organometallics 4 (1985) 1238, and references therein.
[18] J.L. Hughey IV, C.P. Anderson and T.J. Meyer, J. Organomet. Chem. 125 (1977) c49.
[19] G.P. Smith, Polyhedron 7 (1988) 1605.
[20] A. Fox and A. Pöe, J. Am. Chem. Soc. 102 (1980) 2497.
[21] A.F. Hepp and M.S. Wrighton, J. Am. Chem. Soc. 105 (1983) 5934.
[22] I.R. Dunkin, P. Härter and C.J. Shields, J. Am. Chem. Soc. 106 (1984) 7248.
[23] J.D. Simon and X. Xie, J. Phys. Chem. 90 (1986) 6751.
[24] B.O. Roos, in: Proceeding of new challenges in computational quantum chemistry, eds. R. Broer, P.J.C. Aerts and P.S. Bagus, Groningen, Holland (1994).
[25] B. Persson, B.O. Roos and K. Pierloot, J. Chem. Phys. 101 (1994) 6810, and references therein.
[26] A. Veillard and M.-M. Rohmer, Intern. J. Quantum Chem. 42 (1992) 965.
[27] A. Veillard and A. Dedieu, Nouveau J. Chimie 7 (1983) 683.
[28] J. Manz, B. Reischl, T. Schröder, F. Seyl and B. Warmuth, Chem. Phys. Letters 198 (1992) 483; C. Daniel, M.-C. Heitz, J. Manz and C. Ribbing, J. Chem. Phys., in press.
[29] C. Daniel, R. de Vivie-Riedle, M.-C. Heitz, J. Manz and P. Saalfrank, Intern. J. Quantum Chem., in press; 52 (1994) 71.
[30] A.H. Zewail, Femtochemistry – ultrafast dynamics of the chemical bond (World Scientific, Singapore, 1994), and references therein.
[31] S. Leutwyler and U. Even, Chem. Phys. Letters 84 (1981) 188.
[32] J. Opitz and D. Bruch, Intern. J. Mass Spectrom. Ion. Processes 124 (1993) 157.
[33] P.M. Felker and A.H. Zewail, in: Jet spectroscopy and molecular dynamics, eds. M. Hollas and D. Phillips (Chapman and Hall/Blackie, London/London, 1994).
[34] A.H. Zewail, J. Chem. Soc. Faraday Trans. II 85 (1989) 1221.
[35] M.J. Rosker, M. Dantus and A.H. Zewail, J. Chem. Phys. 89 (1988) 6113.